Dynamic Contrast-Enhanced Magnetic Resonance Imaging As a Biomarker for Prediction of Radiation-Induced Neurocognitive Dysfunction

Yue Cao,[1,2] Christina I. Tsien,[1] Pia C. Sundgren,[2] Vijaya Nagesh,[1] Daniel Normolle,[1] Henry Buchtel,[3,5] Larry Junck,[4] and Theodore S. Lawrence[1]

Abstract

Purpose: To determine whether early assessment of cerebral microvessel injury can predict late neurocognitive dysfunction after brain radiation therapy (RT).

Experimental Design: Ten patients who underwent partial brain RT participated in a prospective dynamic contrast-enhanced magnetic resonance imaging (MRI) study. Dynamic contrast-enhanced MRI was acquired prior to, at weeks 3 and 6 during, and 1 and 6 months after RT. Neuropsychological tests were done pre-RT and at the post-RT MRI follow-ups. The correlations between early delayed changes in neurocognitive functions and early changes in vascular variables during RT were analyzed.

Results: No patients had tumor progression up to 6 months after RT. Vascular volumes and blood-brain barrier (BBB) permeability increased significantly in the high-dose regions during RT by 11% and 52% ($P < 0.05$), respectively, followed by a decrease after RT. Changes in both vascular volume and BBB permeability correlated with the doses accumulated at the time of scans at weeks 3 and 6 during RT and 1 month after RT ($P < 0.03$). Changes in verbal learning scores 6 months after RT were significantly correlated with changes in vascular volumes of left temporal ($P < 0.02$) and frontal lobes ($P < 0.03$), and changes in BBB permeability of left frontal lobes during RT ($P < 0.007$). A similar correlation was found between recall scores and BBB permeability.

Conclusion: Our data suggest that the early changes in cerebral vasculature may predict delayed alterations in verbal learning and total recall, which are important components of neurocognitive function. Additional studies are required for validation of these findings.

Radiation therapy (RT) is a major treatment modality for malignant and benign brain tumors. The major limiting factor in its use is neurotoxicity. This neurotoxicity manifests as late neurologic sequelae and neurocognitive dysfunctions with or without gross tissue necrosis (1–4). Late neurocognitive dysfunction prominently affects working memory, learning ability, executive function, and attention span. Although a few studies find that tumor progression is associated with the deterioration of neurocognitive function after RT (5–7), a recent multicenter study of patients with low-grade gliomas who had no clinical signs of tumor recurrence at least 1 year after partial brain (90% of the patients) or whole brain RT showed that a high total dose correlated with a decline in working memory, and that a high dose per fraction interferes with long-term memory storage and retrieval (4). Also, in a randomized trial of low-dose (50.4 Gy) versus high-dose (64.8 Gy) partial brain RT in patients with supratentorial low-grade glioma, significant cognitive deteriorations from baseline were found in those without tumor progression, with rates of 8.2%, 4.6%, and 5.3% at years of 1, 2, and 5, respectively, as assessed by the Folstein Mini-Mental State Examination (MMSE; ref. 8), a relatively crude measure of neurocognitive function. Moreover, the rate of cognitive impairment in patients undergoing partial brain RT is even higher when assessed using a battery of neuropsychological tests that are much more sensitive to cognitive functions than the MMSE (4, 9–12). The potential effect of RT on neurocognitive outcomes is an important factor in the determination of the risks versus benefits of treatment (13), which should be an integral part of clinical decision-making. Given the delayed nature of neurocognitive dysfunction, it would be important to identify biomarkers for early assessment and prediction of late neurotoxicity.

Radiation-induced injury in cerebral tissue is a highly complex and interactive process involving multiple tissue elements (2, 14, 15). Vascular injury has long been considered to be of crucial importance for the development of cerebral tissue toxicity in response to irradiation. A large body of evidence suggests that vascular injury occurs acutely and precedes subacute demyelination and reactive astrocytic and microglial responses (16–19). Early histopathologic changes in

Authors' Affiliations: [1]Radiation Oncology, [2]Radiology, [3]Psychiatry, and [4]Neurology, University of Michigan, Ann Arbor, Michigan, and [5]VA Ann Arbor Healthcare System, Ann Arbor, Michigan

Received 8/11/08; revised 11/24/08; accepted 11/24/08; published OnlineFirst 02/17/2009.

Grant support: 3PO1 CA59827 and R21 CA113699.

The costs of publication of this article were defrayed in part by the payment of page charges. This article must therefore be hereby marked *advertisement* in accordance with 18 U.S.C. Section 1734 solely to indicate this fact.

Requests for reprints: Yue Cao, Departments of Radiation Oncology and Radiology, UH-B2C432, Box 0010, University of Michigan, Ann Arbor, MI 48109-0010. Phone: 734-647-2914; Fax: 734-936-7859; E-mail: yuecao@umich.edu.

doi:10.1158/1078-0432.CCR-08-1420

Translational Relevance

Neurotoxicity is a major clinical complication following radiation therapy of brain tumors. Clinical symptoms can occur acutely and subacutely, but most devastating neurotoxicity manifests with late neurologic sequelae, including neurocognitive dysfunction, white matter degeneration, and necrosis. Late neurocognitive dysfunction presents as diminishing mental capacity for working memory, learning ability, executive function, and attention. Recent multicenter studies of patients with low-grade gliomas who are without clinical signs of tumor recurrence after radiation treatment show that both high total dose as well as high dose per fraction are associated with neurocognitive deterioration, especially related to memory functions. Given the delayed nature of neurocognitive dysfunction, it would be valuable to identify biomarkers, including those derived from *in vivo* imaging, for early assessment of individual sensitivity to radiation and prediction of late neurotoxicity. Such biomarkers might provide an opportunity to individualize the dose of radiation therapy or to begin neuroprotective therapy. This study aims to address this clinically relevant question.

blood vessels after irradiation include dilation and thickening of blood vessels, endothelial cell nuclear enlargement, and hypertrophy of perivascular astrocytes. The dose-dependent endothelial cell death and apoptosis occur as early as 24 hours after irradiation (17, 18). The initial injury of vessels is followed by the formation of platelet matrix and thrombi, which eventually results in occlusion and thrombosis in microvessels within weeks to months (14, 20, 21). Furthermore, cerebral vascular injury is followed by degenerative structural changes in the white matter (22–25). The time lag between vascular injury and demyelination and necrosis in white matter diminishes with increased dose (22). Most of these histopathologic and biological studies have been carried out in rodent models using a single large dose of radiation. Whether the dose-dependent and time-dependent changes in histopathology in the human brain after 5 to 6 weeks of fractionated RT have the same biological sequences has yet to be determined. However, the more serious effects causing neurologic symptoms, including gross white matter necrosis and degeneration, are late effects that generally do not occur until 12 months or more after the completion of RT (1, 2).

Few prospective studies have investigated the effects of radiation on the human brain during a course of radiation and then after treatment over time. One of our previous studies assessed the temporal changes in normal-appearing large white matter fibers longitudinally, and revealed progressive changes beginning early in the course of RT to 9 months after the completion of RT (26). If there are early changes in cerebral vasculature, as has been observed in animal models, and if the early changes in vasculature are associated with late white matter degeneration and/or late neurologic symptoms and neurocognitive dysfunction, then early vascular changes could be a biomarker for late neurotoxicity.

We conducted a prospective study to investigate three questions: (*a*) how cerebral blood vessels in normal tissue of patients who undergo partial brain RT change over time, (*b*) how these changes are related to dose and dose-volume, and (*c*) if these changes are associated with neurocognitive dysfunction. We hypothesized that early monitoring of cerebral blood microvessels in response to fractionated RT would allow the prediction of late neurocognitive deficits. This predictive ability would permit the identification of a time window for neuroprotective therapeutic intervention.

Materials and Methods

Patients. Ten patients with newly diagnosed low-grade glioma, meningioma, cranopharyngioma, or benign tumor underwent three-dimensional conformal cranial RT with a median dose of 54 Gy (range, 50.4-59.4 Gy in 1.8-Gy fractions), and participated in a prospective, Institutional Review Board–approved, clinical magnetic resonance imaging (MRI) study (Table 1). The overall degree of physical function was assessed by using the Karnofsky performance status scale, which was ≥90 prior to RT in all but one patient (who had a Karnofsky score of 80), indicating that these patients were highly functioning.

Dynamic contrast-enhanced MRI. Patients underwent an MRI 1 to 2 wk prior to RT, at wk 2 to 3 and wk 5 to 6 during the course of RT, and at 1 and 6 mo following the completion of RT. All MRI scans were done on a 1.5-T scanner (General Electric Health Care). MRI series included T1-weighted images, T2-weighted fluid-attenuated inversion recovery (FLAIR) images, diffusion tensor images, dynamic contrast-enhanced (DCE) T1-weighted images, post-contrast T1-weighted images, and two-dimensional proton spectroscopy images. DCE images were acquired with a three-dimensional gradient echo pulse

Table 1. Patient demographics, primary diagnosis, and radiation dose

Patient nos.	Age (y)/sex	Diagnosis	Location	Prescribed dose (Gy)	Fraction size (Gy)/no fraction
1	33/M	Grade 2 gemistocytic astrocytoma	Right temporal	59.4	1.8/33
2	64/M	Pituitary macroadenoma	Suprasellar	50.4	1.8/28
3	55/M	Sphenoid wing meningioma	Left medial sphenoid	54.0	1.8/30
4	29/M	Cranopharyngioma	Suprasellar	55.8	1.8/31
5	25/F	Low grade glioma	Left frontal	54.0	1.8/30
6	71/M	Null cell pituitary adenoma	Suprasellar	50.4	1.8/28
7	36/M	WHO III anaplastic supratentorial ependyoma	Left frontal	59.4	1.8/33
8	55/M	Grade 2 astrocytoma	Bifrontal	54.0	1.8/30
9	39/M	Grade 2 mixed oligoastrocytoma	Right frontotemporal	59.4	1.8/33
10	44/M	Pituitary macroadenoma	Suprasellar	50.4	1.8/28

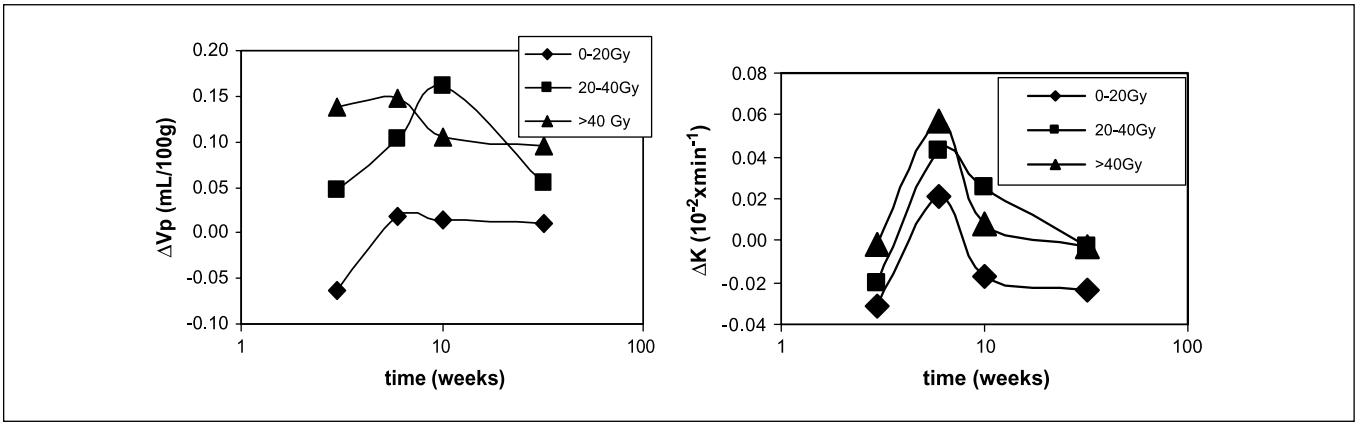

Fig. 1. The differences in the vascular volumes (V_p) and BBB permeability (K^{trans}) in three dose intervals at three observation times compared with the baseline values. In the high-dose region (>40 Gy), the vascular volumes increased significantly at wk 6 during the course of RT and then started decreasing after the completion of RT; whereas in the intermediate dose interval (20-40 Gy), the vessel volume increased slowly, reached a similar maximum value 1 mo after the completion of RT, and then started decreasing. The changes in the BBB permeability were significant in the high and intermediate dose regions at week 6 during the course of RT. 10 wk, 1 mo after the completion of RT; and 32 wk, 6 mo after the completion of RT.

sequence with TE/TR = 1.08/3.4 ms, flip angle = 20 degrees, field-of-view = 220 × 220 × 132 mm^3, matrix size = 256 × 256 × 22, spatial resolution = 0.86 × 0.86 × 6 mm^3, and temporal resolution = 7.2s. The three-dimensional slab was acquired in the sagittal plane to eliminate the time-of-flight effect from in-flow blood proton spins. A total of 38 dynamic volumes were acquired during 274 s. A single dose (0.1 mL/kg) of gadolinium-DTPA was injected at 2 mL/s, during which DCE image volumes were acquired. In this study, we focused on the analysis of DCE images and changes of variables estimated from the DCE data over time.

Image registration. All images including anatomic MRI, DCE-MRI, and treatment planning CT were coregistered by using the Mutual Information and Simplex optimization algorithm implemented in an in-house functional image analysis tool (27). DCE images were first registered within the series to correct possible misalignment prior to estimations of kinetic variables (described in detail below). After estimating kinetic variables, all sagittal parametric maps obtained at different follow-up times were coregistered to the axial post-contrast T1-weighted images acquired prior to RT. Finally, through coregistration of treatment planning CT with MRI, the planned dose distribution map was also coregistered with MRI.

Estimation of kinetic variables from DCE-MRI. The modified Toft model was used to estimate kinetic variables (28). In this model, the variables considered include the transfer constant (K^{trans}) for gadolinium influx from the intravascular space into the extravascular extracellular space, the fractional plasma volume (V_p) in tissue, and the back-flux constant rate for gadolinium efflux from the extravascular extracellular space back to the intravascular space. A small vessel hematocrit value of 0.45 was used. The artery input function was obtained from carotid arteries by thresholding to determine the earliest contrast uptake. Note that the V_p obtained by this model was corrected for vascular leakage.

Temporal change and dose effect. We focused on the temporal change of the fractional volume of blood plasma (V_p) and the transfer constant (K^{trans}) of gadolinium-DTPA from the intravascular space into the extravascular extracellular space in normal-appearing cerebral tissue, which is defined as the cerebral tissue that appears normal on T1-weighted images and FLAIR images from pre-RT to 6 mo after the completion of RT. Changes in K^{trans} reflect changes in blood-brain barrier (BBB) permeability to gadolinium-DTPA. To assess the changes in V_p and K^{trans} in relation to the radiation dose, cerebral tissue was divided into seven intervals based on receiving a biologically equivalent dose of 2 Gy per fraction (biodose, $\alpha/\beta = 2.5$), as 0 to 5, 5 to 10, 10 to 20, 20 to 30, 30 to 40, 40 to 50, and >50 Gy. The means of the biodose in the seven volumes of interest and the means of V_p were calculated. To assess the effect of dose-volume, the brain volumes that received 0 to 20, 20 to 40, and >40 Gy were computed based on the treatment planning CT and dose distribution.

Neurocognitive function tests. All patients underwent a battery of standardized neurocognitive tests prior to RT and at each of the post-RT MRI follow-ups. The neurocognitive tests included Trail Making Tests A and B (29), the Hopkins Verbal Learning Test (HVLT; refs. 30, 31), and the Controlled-Oral Word Association test (32, 33). Trail Making Test A assesses information processing efficiency. Trail Making Test B and Controlled-Oral Word Association assess executive function. HVLT assesses verbal memory (recall, delayed recall, and recognition components) and learning (learning component). In addition, the MMSE was administrated. These neuropsychologic tests were used in Radiation Therapy Oncology Group trials of prophylactic cranial irradiation for patients with limited small cell lung cancer disease (RTOG 0212) and motexafin gadolinium, and whole-brain radiation for patients with brain metastases (5). All tests were administrated by trained and certified research associates for Radiation Therapy Oncology Group trials and standards.

A score of 1.5 SD below the mean of age-matched normative data has been considered to have impairment in neurocognitive function (30, 31). Therefore, if a score of a neurocognitive test in a patient prior to RT was 1.5 SD below the mean of the age-matched normative data, the patient was considered to have pre-existing neurocognitive function impairment.

Statistical methods. The linear mixed model was used to assess the dose effect and the dose-volume effect on the brain vasculature properties of V_p and K^{trans}. First, we tested the dose effect at different time points, during the course of RT and after the completion of RT, to evaluate the evolution of the dose effect over time. The linear mixed model was considered as:

$$\Delta P_{ijt} = \alpha_t + \beta_t \times D_{ijt} + a_{it}, \quad [1]$$

where subscripts i, j, and t denote, respectively, subject, region, and time; ΔP is the change of V_p or K^{trans} observed at time t compared with that patient's baseline; and D_{ijt} is the biologically corrected dose received in region j of subject i by time t. β_t is the slope at time t, and its change over time would suggest the dose effect evolving. α_t and a_{it} are the global intercept and the individual subject intercept at time t, respectively. Second, we tested the dose-volume effect as a possible additional factor contributing to injury of the cerebral vasculature. The model was tested given by

$$\Delta P_{ijt} = \alpha_t + \beta_t \times (D_{ijt} \times V_{ik}) + a_{it}, \quad [2]$$

where V_{ik} is the dose-volume of either $V_{0\text{-}20}$, $V_{20\text{-}40}$, or $V_{>40}$ for patient i. Given that the three dose volumes are correlated, only one dose volume can be added into the model each time.

The correlations between the early changes in V_p and K^{trans} during the course of RT and the early delayed changes (6 mo after RT) in neurocognitive functions were tested by Pearson correlation coefficient. Because we predicted the direction of expected changes, one-tailed $P < 0.05$ was considered to be significant.

Results

Clinical and radiological findings. None of the patients evidenced tumor progression at 6 months (of 10 eligible patients) or 18 months (of 5 eligible patients) after the completion of RT. Also, none of the 10 patients showed gross radiation-induced lesions on T2-weighted FLAIR and post-gadolinium T1–weighted images up to 6 months after RT. All patients with glioma and the patient with ependymoma had associated signal increases on T2-weighted FLAIR images in the tumor and in its vicinity prior to RT. These tumor-related hyperintensities on T2-weighted FLAIR images did not substantially change during the 6-month follow-up. In one patient with glioma, mild scattered focal areas of increased T2/FLAIR signal abnormalities were present in the centrum semiovale and periventricular white matter prior to RT, consistent with old ischemic changes. These areas showed no further change over time. No additional areas of radiation-induced abnormalities were present during follow-up. In patients with pituitary adenomas and in the patient with craniopharyngioma, no signal abnormality outside the tumor was present pretreatment and no interval change was seen during the 6-month follow-up. In the patient with sphenoid wing meningioma, postsurgical changes were shown, and no changes on T2 and FLAIR signals beyond the surgical cavity were seen over the 6-month follow-up.

Temporal changes in vascular volumes and BBB permeability. The averaged fractional volume of blood plasma (V_p; representing the vascular volume when corrected with hematocrit) in normal-appearing cerebral tissue in the patients was 1.4 mL/100 g prior to RT, which is in the reference range. The temporal changes in V_p exhibited a complex pattern in relation to radiation dose variables. First, the temporal changes in V_p were evaluated in three dose intervals as 0 to 20, 20 to 40, and >40 Gy, which have been used in previous studies to assess the dose-volume effect (34). The time courses of the changes in V_p depended on the dose received by the tissue regions (Fig. 1). For the cerebral tissue regions that received the low dose (0-20 Gy), V_p exhibited nonsignificant changes ($P > 0.05$). In the tissue regions that received 20 to 40 Gy, V_p increased by 4% (0.05 ± 0.08 mL/100 g; mean ± SE) at week 3 during RT. The increase reached 7% (0.10 ± 0.05 mL/100 g) at week 6 during RT and by 12% (0.16 ± 0.10 mL/100 g) 1 month after the completion of RT. The increase was significant at week 6 during RT ($P = 0.05$). Then, at 6 months after the completion of RT, V_p decreased from the value observed 1 month after RT and returned to the values of week 3 during RT (Fig. 1), suggesting that in this intermediate dose range, vessels are dilated initially and then either return to normal or undergo regression. In the brain region that received >40 Gy, V_p rapidly increased by 10% (0.14 ± 0.09 mL/100 g) at week 3 during the course of RT, and by 11% (0.15 ± 0.07 mL/100 g) at week 6 during RT, approximately the maximum value observed in the 20 to 40 Gy brain region 1 month after RT. The increase in V_p at week 6 during RT was significant ($P < 0.05$). After the completion of RT, V_p values decreased from the elevated values during RT to the value at 6 months (0.10 ± 0.10 mL/100 g), which was still 7% greater than the baseline value, suggesting that this higher dose range evokes rapid vessel dilation, followed by vessel regression or renormalization after the completion of RT. The transition occurred sooner in the high dose range than the intermediate dose range.

Temporal profiles of the changes in K^{trans} (reflecting BBB permeability to gadolinium-DTPA) of normal-appearing brain were similar to those in V_p (Fig. 1). In the regions which received low doses (0-20 Gy), K^{trans} exhibited nonsignificant changes. In the region that received 20 to 40 Gy, K^{trans} values increased significantly by 39% ($0.042 \pm 0.016\ 10^{-2} \times \text{min}^{-1}$) at week 6 during the course of RT ($P < 0.02$). After the completion of RT, the K^{trans} values started to decrease from the elevated values at the end of RT, but still remained elevated by 23% ($0.025 \pm 0.014\ 10^{-2} \times \text{min}^{-1}$) 1 month post-RT, and eventually returned to the pre-RT values 6 months post-RT. In the tissue region that received >40 Gy, the K^{trans} values increased significantly by 52% ($0.057 \pm 0.019\ 10^{-2} \times \text{min}^{-1}$) at week 6 during the course of RT ($P < 0.01$). After the completion of RT, the K^{trans} values decreased from the elevated values at the end of RT, which is similar to the temporal pattern that we observed previously in the tumor of a different group of patients (35).

Table 2. Linear mixed models

Time	3 wk		6 wk		10 wk		32 wk	
	β_t	*P*	β_t	*P*	β_t	*P*	β_t	*P*
V_p								
Model 1	1.1×10^{-2}	0.0001	4.8×10^{-3}	0.0002	3.6×10^{-3}	0.001		n.s.
Model 2	3.5×10^{-5}	0.0001	1.3×10^{-5}	0.0001	1.3×10^{-5}	0.0001	7.3×10^{-6}	0.007
K^{trans}								
Model 1	2.0×10^{-5}	0.001	7.8×10^{-6}	0.03	6.1×10^{-6}	0.001	4.5×10^{-6}	0.03

NOTE: Model 1 includes dose effects, whereas model 2 includes dose-volume effects. Units of β_t: (mL/100 g) per Gy for model 1 of V_p, per Gy per mL for model 2 of V_p, and per min per Gy for model 1 of K^{trans}. Weeks were counted from the start of RT; 10 wk, 1 mo after the completion of RT; 32 wk, 6 mo after the completion of RT.

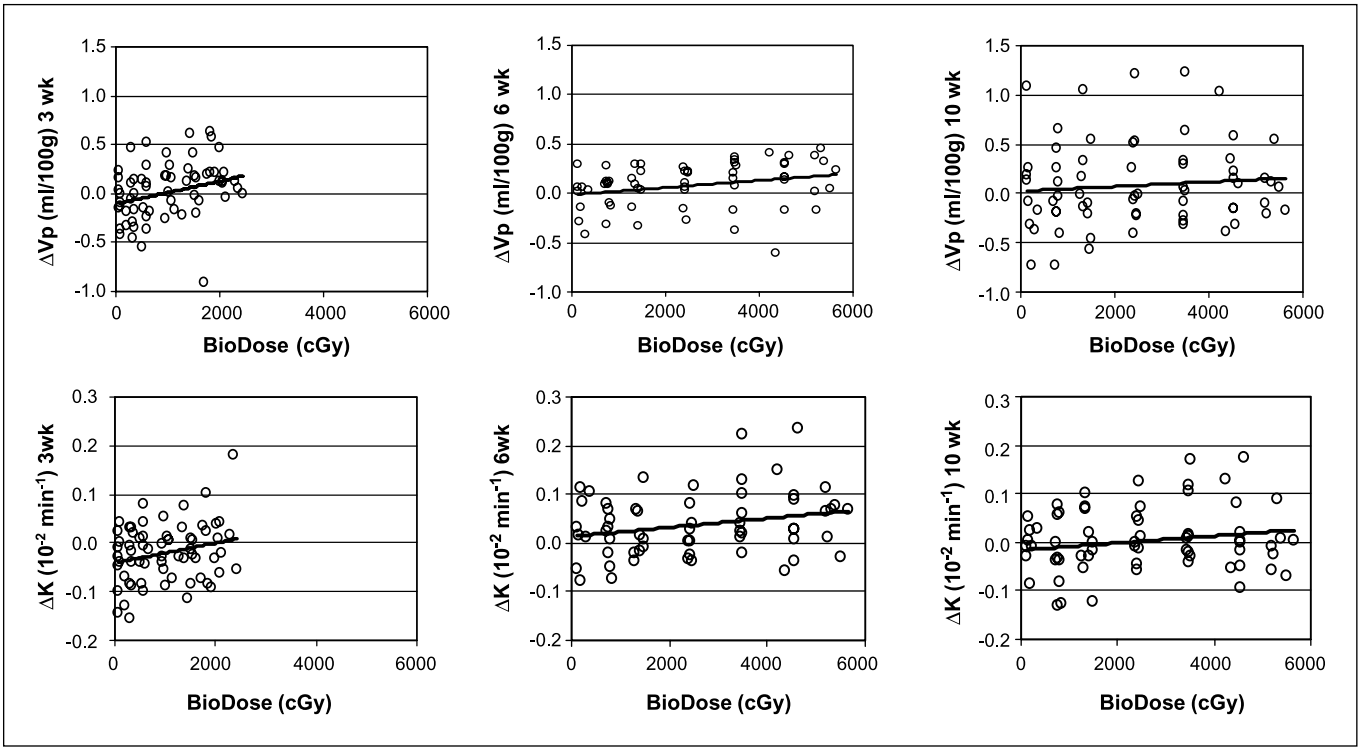

Fig. 2. Scatter plots of the changes in the vascular volumes (V_p, *top*) and blood-brain permeability (K^{trans}, *bottom*) versus doses received at the time of MRI studies. Left, week 3 during RT; middle, week 6 during RT; right, 1 mo after the completion of RT (10 wk from the start of RT). Solid lines, linear regression lines.

Dose effects. The dose effects on the cerebral vasculature were analyzed using the linear mixed model. In model 1 (Eq. A), only the dose effect on the cerebral vasculature and the evolution of the dose-dependency changes over time were examined. The dose-dependence of V_p was the largest at week 3 during the course of RT ($P < 0.0001$; Table 2). At week 6 of RT, the dose-dependence of V_p was high ($P < 0.0001$), but even though the dose received by these tissues was approximately double that at week 3, the dose-dependence of V_p was approximately half of the one observed at week 3 (Table 2). After the completion of RT, the dose-dependent change in V_p continued decreasing, and by 6 months after RT, the dose-dependence of V_p was diminished. This evolution of the dose-dependent changes in V_p can also be seen in the scatter plots of Fig. 2.

Using the linear mixed model, the changes in K^{trans} (BBB permeability to gadolinium-DTPA) both during the course of RT and after the completion of RT were found to depend significantly on the accumulated doses at the time of the MRI observation ($P = 0.001$ to $P = 0.03$; Table 2; Fig. 2). The linear slopes (β_t) that reflect K^{trans} value changes per unit dose were 2.0×10^{-5}, 7.8×10^{-6}, 6.1×10^{-6}, and 4.5×10^{-6} min^{-1}/Gy at week 3 and week 6 during the course of RT and 1 month and 6 months after the completion of RT, respectively, indicating the strongest dose-response at week 3 during RT.

Dose-volume effects. To evaluate whether the volume of brain irradiated affects blood volume in addition to the dose, we developed model 2, which includes the dose-volume effect (Eq. B). The changes in V_p were found to depend on the product of the biodose received at the time of observation and the volume of brain receiving a total dose of >40 Gy ($V_{>40}$), indicating that the effect of higher doses of radiation was greater with increasing brain volume irradiated with the high doses (Table 2). The dose and dose-volume ($D \times V_{>40}$)–dependent changes in V_p were significant both during and after the completion of RT (Table 2). Again, the strongest interactive effect of the dose and the dose-volume on V_p was observed at week 3 during the course of RT, and the effect remained significant 6 months after the completion of treatment ($P < 0.007$; Table 2). There was no significant dose-volume effect on K^{trans} values found using the linear mixed model.

Neurocognitive function changes. All patients had MMSE scores of 27 or above prior to RT, and this measure showed little change over the 6 months after the completion of RT (Table 3). HVLT assesses multiple verbal memory and learning components, e.g., recall, learning, and delayed recall. Scores of total recall (sum of three trials), learning, and delayed recall (20-minute delay) pre-RT, and 1 month and 6 months after the completion of RT are given in Table 3. Prior to RT, the total recall scores of five patients were more than 1.5 SDs below the means of the age-matched normative data; the delayed recall scores of three patients were more than 1.5 SDs below the means of their age-matched normative data, indicating pre-RT existing conditions in several of the patients. Three patients had borderline impaired learning scores, approximately 1.5 SD below the means of the age-matched normative data, indicating that pre-RT memory abilities were more compromised than learning abilities in these patients in terms of both severity and frequency.

Next, we tested the association between early changes in V_p and K^{trans} during the course of RT and early delayed changes (6 months after the completion of RT) in HVLT recall, learning,

and delayed recall scores. We found that the changes in the verbal learning scores 6 months after RT compared with pre-RT were correlated significantly with the percentage of changes in V_p of left frontal lobes ($P = 0.032$) and left temporal lobes ($P = 0.017$) at week 3 during the course of RT (Fig. 3). There was no significant correlation between the early delayed changes in learning scores and the early changes in V_p of right frontal or temporal lobes, consistent with presumed left hemisphere predominance for language and therefore for verbal learning. The declines in verbal learning scores 6 months after RT versus pre-RT were significantly correlated with the percentage of changes in K^{trans} of left frontal lobes at week 3 during the course of RT ($P = 0.007$), but not with the changes in K^{trans} of right frontal lobes or left and right temporal lobes at week 3 during RT. There was no significant correlation between the early delayed changes in total recall or delayed recall scores and the early changes in V_p during the course of RT of left or right frontal or temporal lobes. The changes in total recall scores 6 months after RT were significantly correlated with the percentage of changes in K^{trans} of left temporal lobes ($P = 0.028$) at week 3 during the course of RT. There was no significant correlation between the early delayed changes in Trail Making Test B or Controlled-Oral Word Association test and the early changes in V_p or K^{trans} during the course of RT of left or right frontal or temporal lobes.

Discussion

In this study, we assessed the early vascular changes during the course of RT and the changes that occurred up to 6 months after the completion of RT. The vascular volume and BBB permeability showed an initial increase during the course of RT, and then a gradual decrease after the completion of RT. The regions receiving the highest doses showed the most rapid and significant changes. The initial increase in vascular volume is most likely due to vessel dilation in response to accumulated modest amounts of radiation (14, 15, 17, 22, 23). The early delayed decrease represents either vascular regression such as capillary collapse and occlusion after progressive loss of endothelial cells and formation of platelet clusters and thrombi (14, 17, 18, 21) or vessel renormalization. The temporal profile of the changes in BBB permeability of normal tissue is similar to what we have observed previously in the tumor of a different patient population (35). The increase in BBB permeability could be due to endothelial cell death and apoptosis in response to irradiation, which is directly correlated to the dose. However, the dose effect on the cerebral vasculature volume is observed during the course of RT, and then diminishes over time after the completion of RT, whereas the dose-volume effect persists up to 6 months after RT. This evolution from the dose effect to the dose-volume effect has not previously been shown. Finally, these early changes (week 3 during the course of RT) in the cerebral vascular volume and BBB permeability are associated with the early delayed changes in learning and recall scores of HVLT. These findings suggest that early changes in the cerebral vasculature may predict delayed changes in verbal learning and total recall, which are key components in neurocognitive function. Additional studies are required for the validation of these findings.

Our understanding of the histopathologic and biological changes in cerebral vasculature and tissue after RT is derived mainly from the studies of rodent models. Most of these studies have been carried out by using a single dose of modest to high size, although some recent studies have used fractionated radiation (21, 36). One such study that used 2 Gy per fraction, for a total of 40 Gy over 4 weeks in mice, found no early BBB disruption until 90 days after the completion of fractionated irradiation (36). In the present study, we found early vascular changes including the vessel volume and BBB disruption, in which the most apparent changes were seen in the brain regions that received >40 Gy. Nevertheless, several studies of rodent models report early vascular changes after a single dose (17, 18); the time course of progressive injury of cerebral tissue in these models differs somewhat from what we observed in humans who received fractionated RT (2, 14, 15, 22). In clinical studies, T2 lesions are located predominantly in periventricular regions, indicating demyelination, and start appearing 2 to 6 months after RT. The T2 lesions increase over the next year. Necrosis does not occur until a year after RT. In the rodent models, a commonly observed pattern of cerebral tissue injury begins with early vascular injury as vessel dilation and endothelial apoptosis and cell death, progresses to subacute

Table 3. MMSE and HVLT scores

Patient nos.	MMSE (pre-RT, 1m, 6m)	HVLT total recall (pre-RT, 1m, 6m)	HVLT learning (pre-RT, 1m, 6m)	Delayed recall (pre-RT, 1m, 6m)
1	30, 30, 30	26, 25, 34	3, 4, 2	9, 10, 11
2	27, 27, 28	17,* 23, 29	4, 5, 6	9, 10, 9
3	28, 26, 29	5,* 14, 13	1,† 2, 1	0,* 2, 1
4	30, 30, 30	33, 26, 25	3, 6, 3	12, 12, 12
5	29, 30, 30	28, 29, 28	5, 6, 3	12, 12, 12
6	27, 26, 28	16,* 17, 15	3, 0, 4	5, 5, 6
7	28, 30, 30	29, 24, 30	3, 4, 4	8, 7, 11
8	29, 27, 27	19,* 26, 14	1,† 3, 3	7,* 9, 5
9	30, 30, 29	26, 21, 23	1,† 2, 3	8, 6, 9
10	30, 29, 29	23,† 22, 19	4, 3, 3	7,* 7, 7

NOTE: Maximum score of MMSE = 30; maximum score for total recall = 36; maximum score delayed recall = 12.
Abbreviations: 1m, 1 mo post-RT; 6m, 6 mo post-RT.
*Score is <1.5 SD below the mean of the age-matched normative data.
†Score is equal to 1.5 SD below the mean of the age-matched normative data (borderline value).

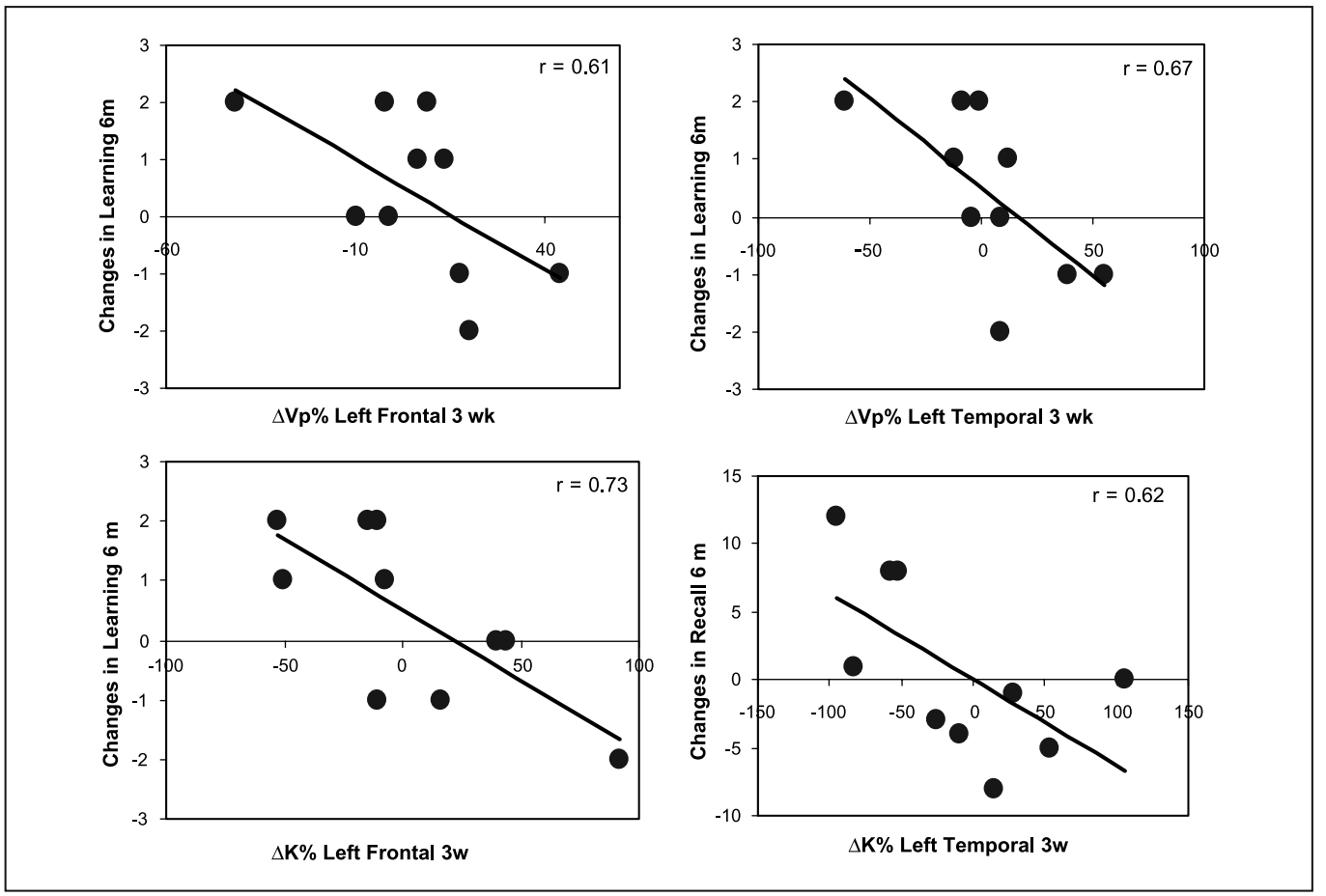

Fig. 3. Correlations between the changes in learning scores 6 mo after RT and the changes in V_p of left frontal (*top left*) and temporal (*top right*) lobes at week 3 during RT, between the changes in learning scores 6 mo after RT and the changes in K^{trans} of left frontal lobes at week 3 during RT (*bottom left*), and between the changes in total recall scores 6 mo after RT and the changes in K^{trans} of left temporal lobes at week 3 during RT (*bottom right*).

demyelination, and is followed by vessel thrombi and diminution, diffuse demyelination, and necrosis. The major discrepancy between clinical observations and rodent models seems to be a lack of the equivalence of the doses to produce similar symptoms. Given that it is extremely difficult to obtain human brain samples to study cerebral normal tissue injury after RT, we must continue to rely on animal models including rodents to understand the histopathology and biology of radiation-induced neurotoxicity. However, extrapolating findings from animal models to humans needs to be done with caution.

The radiation dosimetry variables such as total dose, fraction size, and dose-volume distribution, affect late brain tissue degeneration and neurologic and neurocognitive sequelae in a complex fashion. Our knowledge of the dose-volume effect on the human brain is derived primarily from the reports of late neurologic sequelae and neurocognitive dysfunctions of long-term survivors who have undergone whole brain radiation (3, 9). However, the effect of dose-volume distribution on cerebral tissue injury and neurocognitive outcomes is less clear for partial brain irradiation. Recent efforts have been made to develop statistical models to determine the dose-volume distribution in relation to children's IQ scores months and years after cranial irradiation treatment (34). In the present study, we found that high dose had a greater effect in the patient in whom a large volume of the brain received the high dose. Our preliminary findings indicate that reducing the volume of the brain that receives high doses, e.g., by intensity-modulated RT, may benefit the patients who have a reasonable prospect for long-term survival.

It has been recognized in recent years that the radiation doses below the threshold of causing tissue neurosis poses risks for a patients' cognitive functions years after cranial irradiation (4, 8). For instance, the vascular changes after partial rodent brain irradiation by doses both above and below the threshold of necrosis are associated with impairments of cognitive functions, whereas the low dose affects cognitive functions to a lesser extent (37). In the present study, we show the association between early vascular changes and early delayed neurocognitive function changes in patients who received 50.4 to 59.4 Gy at 1.8 Gy per fraction, in whom no radiation-induced necrosis or white matter abnormality were observed on conventional MRI up to 6 months after RT. Patient variations in tumor locations most likely contribute to neurocognitive abnormalities prior to RT and possibly after RT. In our patients, the verbal learning scores of HVLT prior to RT ranged from borderline deficient to normal and were less compromised by the pre-RT conditions than total recall and

delayed recall. There were consistent correlations between the early delayed changes in learning scores and the early changes in the two vascular variables. It is important to point out that the changes in learning, total recall, and delayed recall scores 6 months after RT were not correlated with the dose, the dose-volume, or the interaction of the dose and dose-volume in either left or right frontal or temporal lobes ($P > 0.5$; data not shown), suggesting that dosimetric variables may not be good surrogates for late delayed neurocognitive function outcomes. This is primarily due to individual sensitivity to radiation, which is not accounted for in the dosimetric variables. A better prediction for the delayed clinical symptoms and neurocognitive outcomes may be gained from assessing individual patient responses to radiation. In one of our recent works, we showed that substantial differences exist between individual patients in the sensitivity of the liver to radiation (38). Assessing individual risks for brain injury after irradiation using functional imaging could allow us to develop individualized patient treatment strategies, which would likely improve outcomes and patient quality of life.

Disclosure of Potential Conflicts of Interest

No potential conflicts of interest were disclosed.

Acknowledgments

The authors thank Kristin Brierley for coordinating the study, Diana Li for data management, and Zhou Shen for programming support.

References

1. Schultheiss TE, Kun LE, Ang KK, Stephens LC. Radiation response of the central nervous system. Int J Radiat Oncol Biol Phys 1995;31:1093–112.
2. Tofilon PJ, Fike JR. The radioresponse of the central nervous system: a dynamic process. Radiat Res 2000;153:357–70.
3. Khuntia D, Brown P, Li J, Mehta MP. Whole-brain radiotherapy in the management of brain metastasis. J Clin Oncol 2006;24:1295–304.
4. Klein M, Heimans JJ, Aaronson NK, et al. Effect of radiotherapy and other treatment-related factors on mid-term to long-term cognitive sequelae in low-grade gliomas: a comparative study. Lancet 2002; 360:1361–8.
5. Mehta MP, Shapiro WR, Glantz MJ, et al. Lead-in phase to randomized trial of motexafin gadolinium and whole-brain radiation for patients with brain metastases: centralized assessment of magnetic resonance imaging, neurocognitive, and neurologic end points. J Clin Oncol 2002;20:3445–53.
6. Meyers CA, Brown PD. Role and relevance of neurocognitive assessment in clinical trials of patients with CNS tumors. J Clin Oncol 2006;24:1305–9.
7. Armstrong CL, Goldstein B, Shera D, Ledakis GE, Tallent EM. The predictive value of longitudinal neuropsychologic assessment in the early detection of brain tumor recurrence. Cancer 2003;97:649–56.
8. Brown PD, Buckner JC, O'Fallon JR, et al. Effects of radiotherapy on cognitive function in patients with low-grade glioma measured by the Folstein Mini-Mental State Examination. J Clin Oncol 2003;21: 2519–24.
9. Roman DD, Sperduto PW. Neuropsychological effects of cranial radiation: current knowledge and future directions. Int J Radiat Oncol Biol Phys 1995;31: 983–98.
10. Postma TJ, Klein M, Verstappen CC, et al. Radiotherapy-induced cerebral abnormalities in patients with low-grade glioma. Neurology 2002;59:121–3.
11. Crossen JR, Garwood D, Glatstein E, Neuwelt EA. Neurobehavioral sequelae of cranial irradiation in adults: a review of radiation-induced encephalopathy. J Clin Oncol 1994;12:627–42.
12. Armstrong CL, Hunter JV, Ledakis GE, et al. Late cognitive and radiographic changes related to radiotherapy: initial prospective findings. Neurology 2002; 59:40–8.
13. Mulhern RK, Palmer SL, Merchant TE, et al. Neurocognitive consequences of risk-adapted therapy for childhood medulloblastoma. J Clin Oncol 2005;23: 5511–9.
14. Belka C, Budach W, Kortmann RD, Bamberg M. Radiation induced CNS toxicity-molecular and cellular mechanisms. Br J Cancer 2001;85:1233–9.
15. Wong CS, Van der Kogel AJ. Mechanisms of radiation injury to the central nervous system: implications for neuroprotection. Mol Interv 2004;4:273–84.
16. Price RE, Langford LA, Jackson EF, Stephens LC, Tinkey PT, Ang KK. Radiation-induced morphologic changes in the rhesus monkey (*Macaca mulatta*) brain. J Med Primatol 2001;30:81–7.
17. Ljubimova NV, Levitman MK, Plotnikova ED, Eidus L. Endothelial cell population dynamics in rat brain after local irradiation. Br J Radiol 1991;64:934–40.
18. Pena LA, Fuks Z, Kolesnick RN. Radiation-induced apoptosis of endothelial cells in the murine central nervous system: protection by fibroblast growth factor and sphingomyelinase deficiency. Cancer Res 2000;60:321–7.
19. Li YQ, Chen P, Haimovitz-Friedman A, Reilly RM, Wong CS. Endothelial apoptosis initiates acute blood-brain barrier disruption after ionizing radiation. Cancer Res 2003;63:5950–6.
20. Verheij M, Dewit LG, Boomgaard MN, Brinkman HJ, van Mourik JA. Ionizing radiation enhances platelet adhesion to the extracellular matrix of human endothelial cells by an increase in the release of von Willebrand factor. Radiat Res 1994;137:202–7.
21. Brown WR, Thore CR, Moody DM, Robbins ME, Wheeler KT. Vascular damage after fractionated whole-brain irradiation in rats. Radiat Res 2005;164: 662–8.
22. Reinhold HS, Calvo W, Hopewell JW, van der Berg AP. Development of blood vessel-related radiation damage in the fimbria of the central nervous system. Int J Radiat Oncol Biol Phys 1990;18:37–42.
23. Calvo W, Hopewell JW, Reinhold HS, Yeung TK. Time- and dose-related changes in the white matter of the rat brain after single doses of X rays. Br J Radiol 1988;61:1043–52.
24. Okeda R, Okada S, Kawano A, Matsushita S, Kuroiwa T. Neuropathology of delayed encephalopathy in cats induced by heavy-ion irradiation. J Radiat Res (Tokyo) 2003;44:345–52.
25. Fike JR, Sheline GE, Cann CE, Davis RL. Radiation necrosis. Prog Exp Tumor Res 1984;28:136–51.
26. Nagesh V, Tsien CI, Chenevert TL, et al. Radiation-induced changes in normal-appearing white matter in patients with cerebral tumors: a diffusion tensor imaging study. Int J Radiat Oncol Biol Phys 2008;70: 1002–10.
27. Cao Y. Development of image software tools for radiation therapy assessment. Med Phys 2005;32: 2136.
28. Tofts PS, Brix G, Buckley DL, et al. Estimating kinetic parameters from dynamic contrast-enhanced T(1)-weighted MRI of a diffusable tracer: standardized quantities and symbols. J Magn Reson Imaging 1999;10:223–32.
29. Tombaugh TN. Trail Making Test A and B: normative data stratified by age and education. Arch Clin Neuropsychol 2004;19:203–14.
30. Benedict RH, Zgaljardic DJ. Practice effects during repeated administrations of memory tests with and without alternate forms. J Clin Exp Neuropsychol 1998;20:339–52.
31. Benedict RHB, Schretlen D, Groninger L, Brandt J. Hopkins Verbal Learning Test—revised: normative data and analysis of inter-form and test-retest reliability. Clin Neuropsychologist 1998;12:43–55.
32. Lezak MD. Neuropsychological assessment. New York: Oxford University Press; 1995.
33. Spreen O, Strauss E, A compendium of neuropsychological tests. New York: Oxford University Press; 1998.
34. Merchant TE, Kiehna EN, Li C, Xiong X, Mulhern RK. Radiation dosimetry predicts IQ after conformal radiation therapy in pediatric patients with localized ependymoma. Int J Radiat Oncol Biol Phys 2005;63: 1546–54.
35. Cao Y, Tsien CI, Shen Z, et al. Use of magnetic resonance imaging to assess blood-brain/blood-glioma barrier opening during conformal radiotherapy. J Clin Oncol 2005;23:4127–36.
36. Yuan H, Gaber MW, Boyd K, Wilson CM, Kiani MF, Merchant TE. Effects of fractionated radiation on the brain vasculature in a murine model: blood-brain barrier permeability, astrocyte proliferation, and ultrastructural changes. Int J Radiat Oncol Biol Phys 2006;66: 860–6.
37. Hodges H, Katzung N, Sowinski P, et al. Late behavioural and neuropathological effects of local brain irradiation in the rat. Behav Brain Res 1998;91:99–114.
38. Cao Y, Pan C, Balter JM, et al. Liver function after irradiation based on computed tomographic portal vein perfusion imaging. Int J Radiat Oncol Biol Phys 2008;70:154–60.